Supporting Information
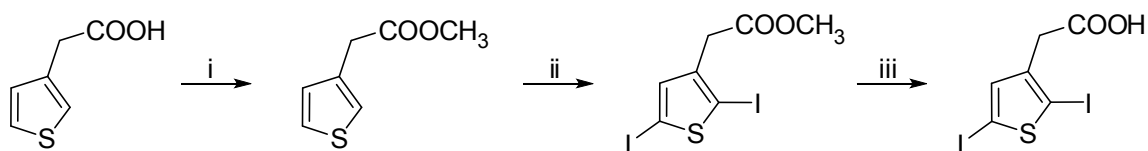
Acetylcholinesterase-Induced Fluorescence Turn-Off of an Oligothiophene-Grafted Quartz Surface Sensitive to Myristoylcholine

G. Grisci, W. Mróz, U. Giovanella, K. Pagano, W. Porzio, L. Ragona,* F. Samperi, S. Tomaselli, F. Galeotti* and S. Destri

1. Synthesis of the di-iodinated thiophene monomer

(i) H_2SO_4, MeOH, reflux, 24 h; *(ii)* *N*-iodosuccinimide, $CHCl_3$/CH_3COOH 1:1, rt, 18 h; *(iii)* 1N $NaOH_{aq}$, THF, rt.

Scheme 1S. Reaction scheme for 2-(2,5-Diiodothiophen-3-yl)acetic acid.

2. ¹H NMR Characterization of AA-OT

¹H NMR spectrum of AA-OT in DMSO-d_6 (Figure 1S) displays the distinctive resonance due to the proton of carboxylic groups at 12.71 ppm along with a relatively confused mix of sharp and well-framed signals overlapping with broader components both in the aromatic region (~ 6.80-7.95 ppm) and in down-field aliphatic region (~ 3.60-4.00 ppm). We ascribed this to the presence of oligomer species showing both different lengths and diverse regiorandom enchainment. Specifically, by comparing this ¹H NMR spectrum with those of the building blocks used to assemble AA-OT, doublets-like components clearly emerging on the two sides of the crowded aromatic range were attributed to H-2 and H-6 of *p*-phenyl end system (6.84 and 7.08 ppm) and to H-δ of terminal thiophene ring (7.67 and 7.77 ppm). No residual signals of unreacted monomers and end-capping agents were found.
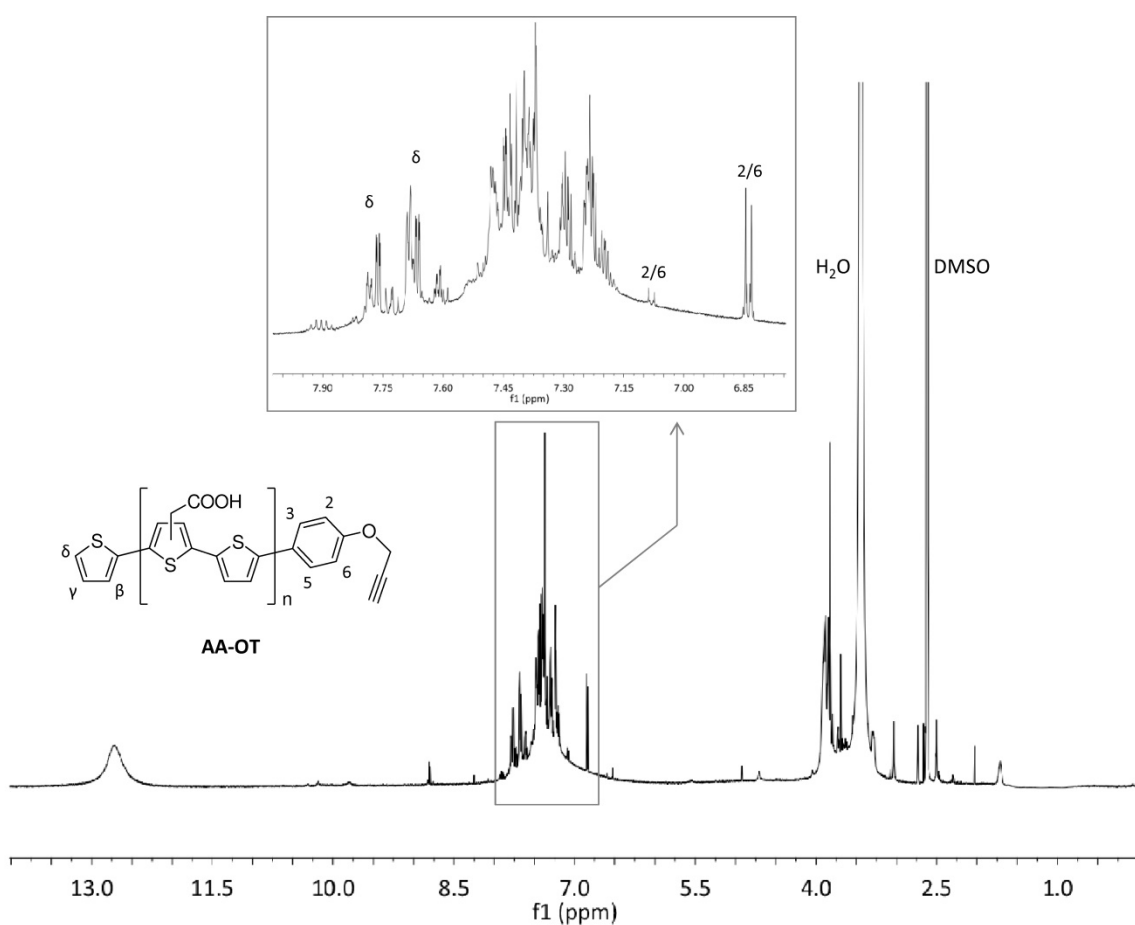
Figure 1S. ¹H NMR spectrum (600 MHz) of AA-OT in DMSO-d_6.

3. MALDI-TOF Mass Spectroscopy

The best mass spectra were recorded using HABA as the matrix. Figure 2S shows a typical spectrum obtained in linear mode with a mass resolution of about 1500 (M/ΔM). The most intense peaks are attributable to species terminated with the expected end-groups. In particular, the presence of the propargyl ending functionality, which is crucial for the subsequent grafting through the CuAAC click chemistry reaction, is confirmed for in most of the analyzed fragments. Most of the recorded *m/z* peaks are attributable to the [M+K]⁺ ion, due to the trace of potassium ions present in the matrix and in the neat sample. All the other lower signals can be related to undesired products originated by the side reactions, *e.g.* deiodination and deboronation. In Figure 2S, the chemical structures likely corresponding to the most intense peaks are reported, together with their calculated molecular weight. Each peak refers to a mixture of isomers. For the sake of clarity only the regioregular isomer structure is shown, and potassium substitution is arbitrary attributed to one of the –COOH groups. The corresponding *n* value is indicated above each structure, where *n* is the number of constitutional repeating units. As evidenced, the longest detected oligomer has *n* = 4, meaning eight thiophene rings plus clickable end-capper.
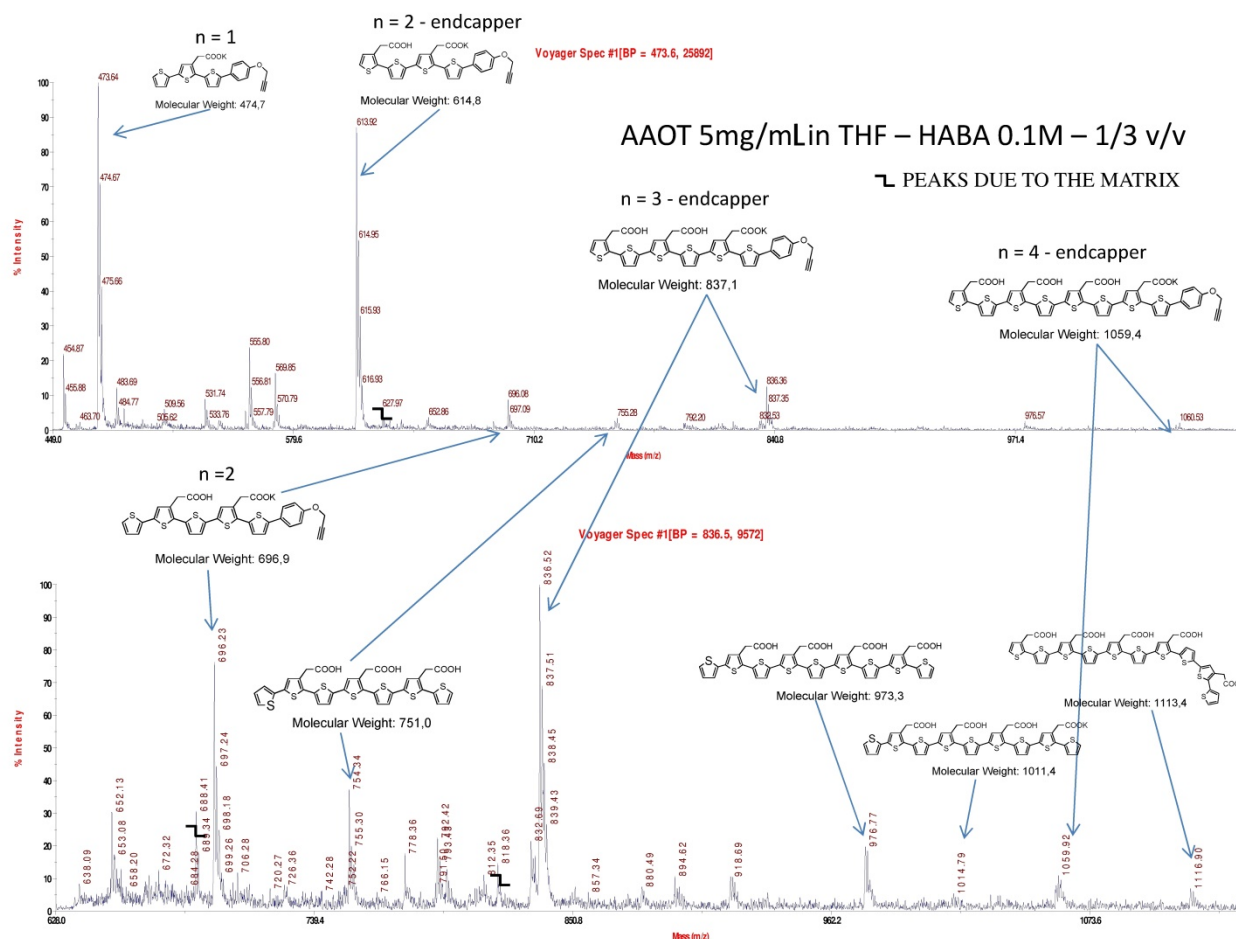
Figure 2S. Positive ions MALDI-TOF mass spectroscopy analysis of AA-OT recorded in linear mode using HABA as a matrix.

The mass spectra measured in reflectron mode shows the same peaks observed in the spectra recorded in linear mode, but with a higher resolution so as to observe the isotopic distribution of peaks as highlighted in Figure 3S. The isotopic distributions of each mass peaks corresponding to the oligothiophenes reported in Figure 2S match very well with their theoretical distribution, as well as for the potassiated ions at *m/z* 614.5 displayed in the Inset of Figure 3S. This data confirm the assignments summarized in the aforementioned Figure 2S. In both spectra the most intense peaks are accompanied of ancillary peaks at *m/z* less of 44 due to

the ions formed owing to the decarboxylation processes occurring in the MALDI analysis condition. These peaks are labeled with the symbol *.
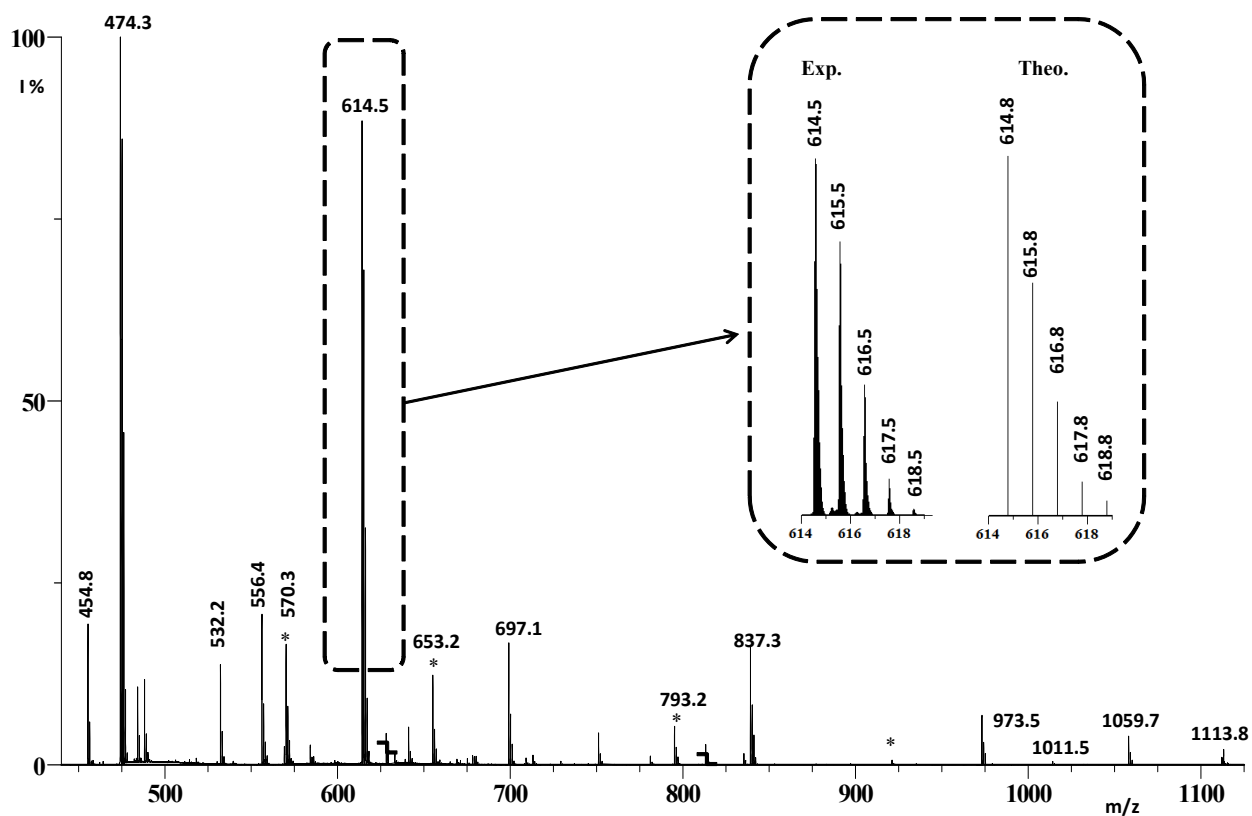

Figure 3S. Positive ions MALDI-TOF mass spectrum of AA-OT recorded in reflectron mode using HABA as a matrix.

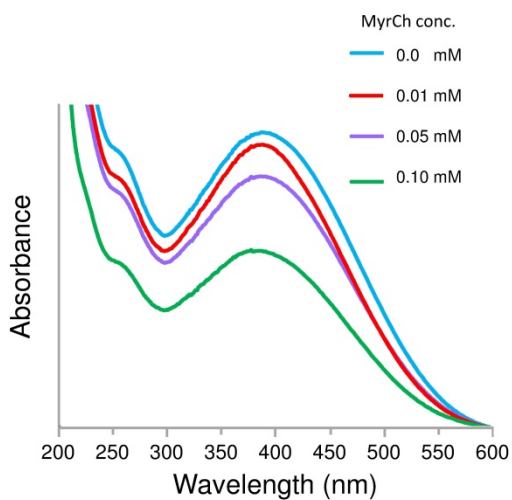## 4. Optical Characterization

Figure 4S. UV-vis absorption spectra of AA-OT 0.45 mM solutions in PB (pH 8) containing different amounts of MyrCh.

5. NMR characterization of AA-OT aggregation state and interactions upon addition of Myristoylcholine (MyrCh) or Choline (Ch)

As shown in Figure 5S B, the absence of changes in AA-OT chemical shifts and diffusion values upon choline addition, as observed from ¹H 1D and DOSY spectra, respectively (Figure 5S), suggest that Ch is not able to dissociate AA-OT aggregates as efficiently as observed for MyrCh.
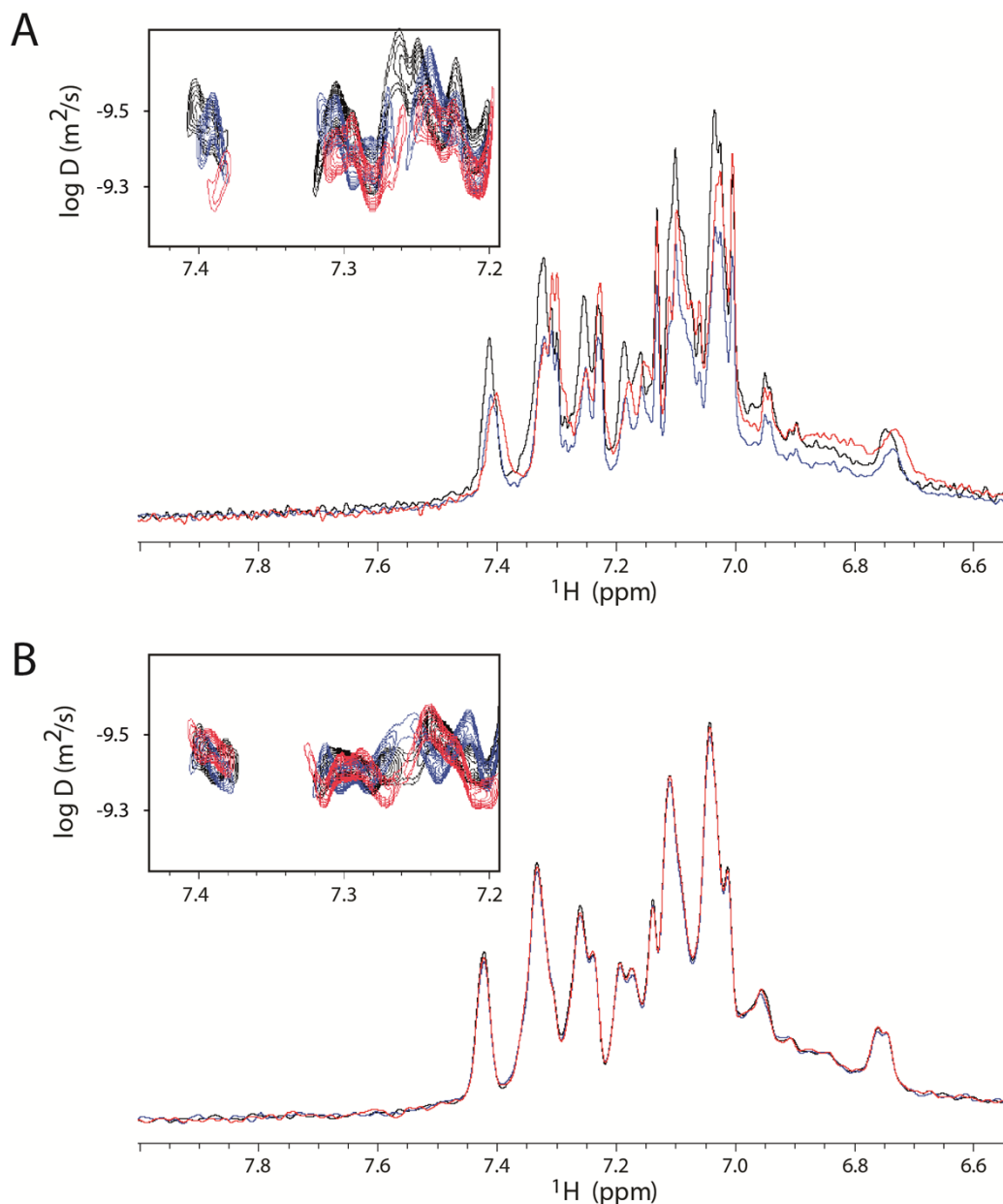
Figure 5S. A) Overlay of ¹H 1D spectra of AA-OT in the presence of MyrCh at 0 (black), 0.1 (blue), and 0.2 (red) MyrCh:AA-OT molar ratios, at 25 °C. Aromatic resonances region is displayed. The inset shows the overlay of the corresponding 2D DOSY spectra with the same color code. Spectra were acquired at 600 MHz DMX Bruker spectrometer. B) Overlay of ¹H 1D spectra of AA-OT in the presence of Ch at 0 (black), 0.1 (blue), and 0.2 (red) Ch:AA-OT molar ratios, at 25 °C. Aromatic resonances region is displayed. The inset shows the overlay of the corresponding 2D DOSY spectra with the same color code. Spectra were acquired at 500 MHz DMX Bruker spectrometer.

## 6. Quartz surface modification with propargyl-rhodamine B model molecule

As a model molecule for AA-OT, we chose a propargyl derivative of the highly fluorescent dye rhodamine B (Figure 6S C), so to be able to easily evaluate the success of the grafting by fluorescence microscopy, and to optimize the reaction conditions for AA-OT grafting. After treatment (Scheme 2S), the slides were rinsed with different solvents until the disappearance of the rhodamine B emission peak from the washing solutions. In Figure 6S, frames A and B show the grafted quartz surface by optical and fluorescence microscopy, while the comparison between PL spectra of the pristine quartz (black curve) and click-grafted quartz (red curve) is displayed in frame D.
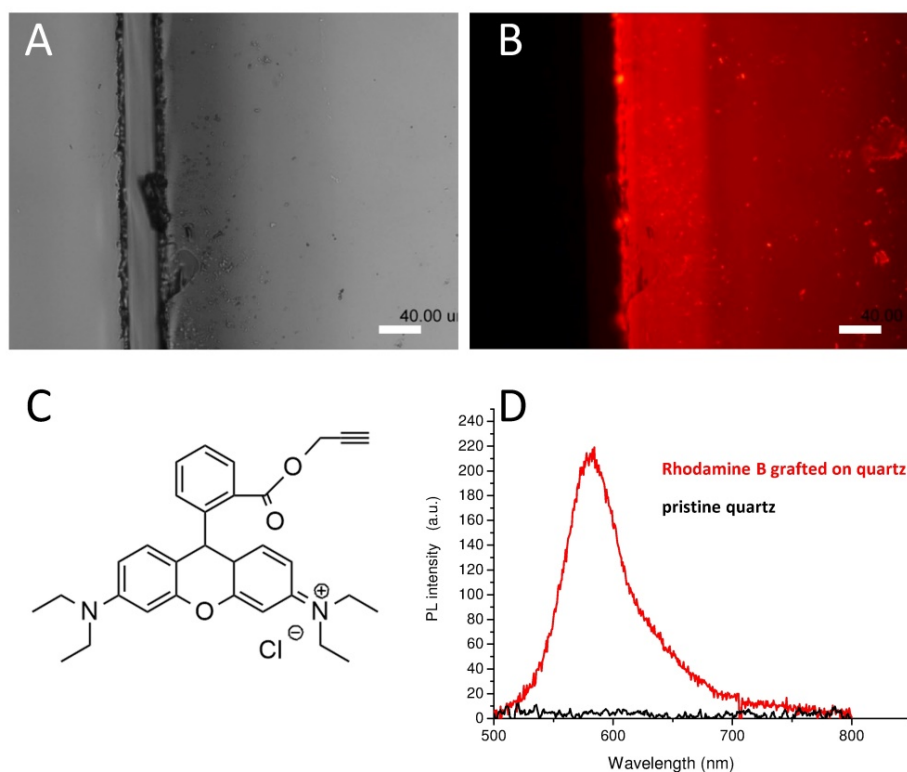
Figure 6S. A) Direct comparison between pristine (left) and grafted (right) quartz substrates seen by optical microscope. B) Same view taken in fluorescence microscopy. The pristine substrate appears dark while the rhodamine grafted surface appears bright red. The scale bar is 40 μm. C) Chemical structure of the clickable rhodamine B derivative. D) PL spectra of pristine quartz surface (black) and rhodamine B grafted quartz (red).

The azido-modified quartz surface was prepared as reported in the experimental section of the paper (see article text). Here, we only described the last step, *i.e.* the CuAAC-based grafting of propargyl-rhodamine B model molecule on quartz slides.

In a 4.0 mL capped vial equipped with a magnetic stir bar, a solution of propargyl-rhodamine B (~ 2.0 mM) in THF (1.5 mL) was stirred at room temperature for 1 h. Then, *N,N*-diisopropylethylamine (DIPEA, 0.001 mL) and a catalytic amount of CuI were added. Thereafter, the substrates were taken from the solution and rinsed in sequence with plenty of fresh THF, 28-30% NH_4OH_{aq}, 1N HCl_{aq}, ultrapure water (MilliQ, ρ ~ 18.2 MΩ cm at 25 °C), EtOH and CH_2Cl_2 to remove any physisorbed contaminants. The quartz surface-grafted rhodamine B samples were dried under a nitrogen stream and finally kept under inert atmosphere for further characterization.
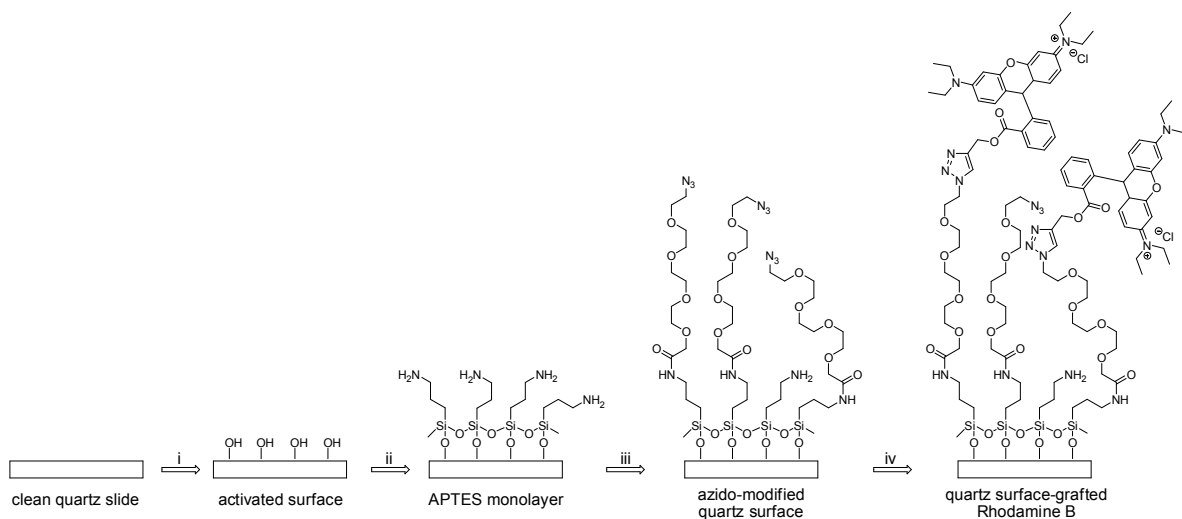
(i) 96% H_2SO_4/35% H_2O_2 (3:1 v/v), rt, 30 min; *(ii)* APTES, dry toluene, rt, 4 h; *(iii)* OEG-4, EDC·HCl, DMAP, TEA, CH_2Cl_2, rt, 24 h; *(iv)* Propargyl-rhodamine B, CuI, DIPEA, THF, rt, 24 h.

Scheme 2S. Synthetic approach for grafting propargyl-rhodamine B model molecule on quartz slides via CuAAC.

7. Surface analysis of quartz functionalization with AA-OT

7.1. Contact angle measurement

We studied the hydrophilicity of quartz surface before and after the different functionalization steps by contact angle (θ) measurement. As shown in Figure 7S, all samples have contact angles smaller than 90°. As a consequence of APTES functionalization, a clear increment of the surface wettability, with θ value passing from 82 to 69°, is observed. By the further OEG_4-N_3 grafting step, the wettability is again slightly increased, because of the presence of the hydrophilic OEG chain. Finally, the last AA-OT grafting step, does not affect greatly the contact angle, even though a slight depletion of the wettability is observed.
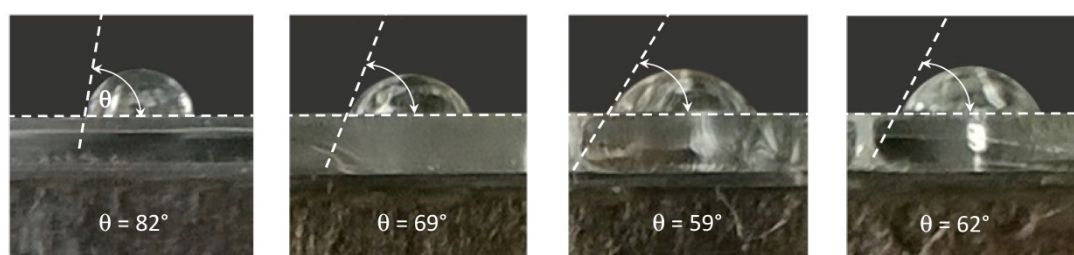

Figure 7S. Profile of water droplets on quartz surface at different grafting steps, from nude quartz to AA-OT brush and determination of water contact angle (θ).

7.2. AFM analysis

We investigated further the quartz surface modifications during each grafting-onto step, by studying the morphology using tapping-mode AFM. In Figure 8S, the morphology of pristine quartz substrate, after treatment with APTES, after OEG_4-N_3 functionalization and after AA-OT click reaction, is shown.
Both 5×5 (first row) and 1×1 μm scans reveal a gradual roughness increase with the progress of the grafting-onto procedure. At the same time, the veining clearly observable in the pristine quartz becomes gradually

less evident, because of the presence of the grafted layers. As shown in the plot reported in Figure 9S, the RMS roughness (measured on the 5×5 µm scans) increases only slightly after the APTES surface reaction, as expected for a SAM of limited molecular length, while for the further two steps a marked roughness enhancement is observed. In particular, RMS roughness increases from 0.56 to 0.96 nm after reaction of OEG$_4$ spacer on the APTES functionalized surface, and from 0.96 to 1.43 nm after the click reaction with AA-OT. The very limited differences in phase contrast observed in the images reported in the last row of Figure 8S confirm that the organic layer covering the quartz substrate is rather homogeneous.
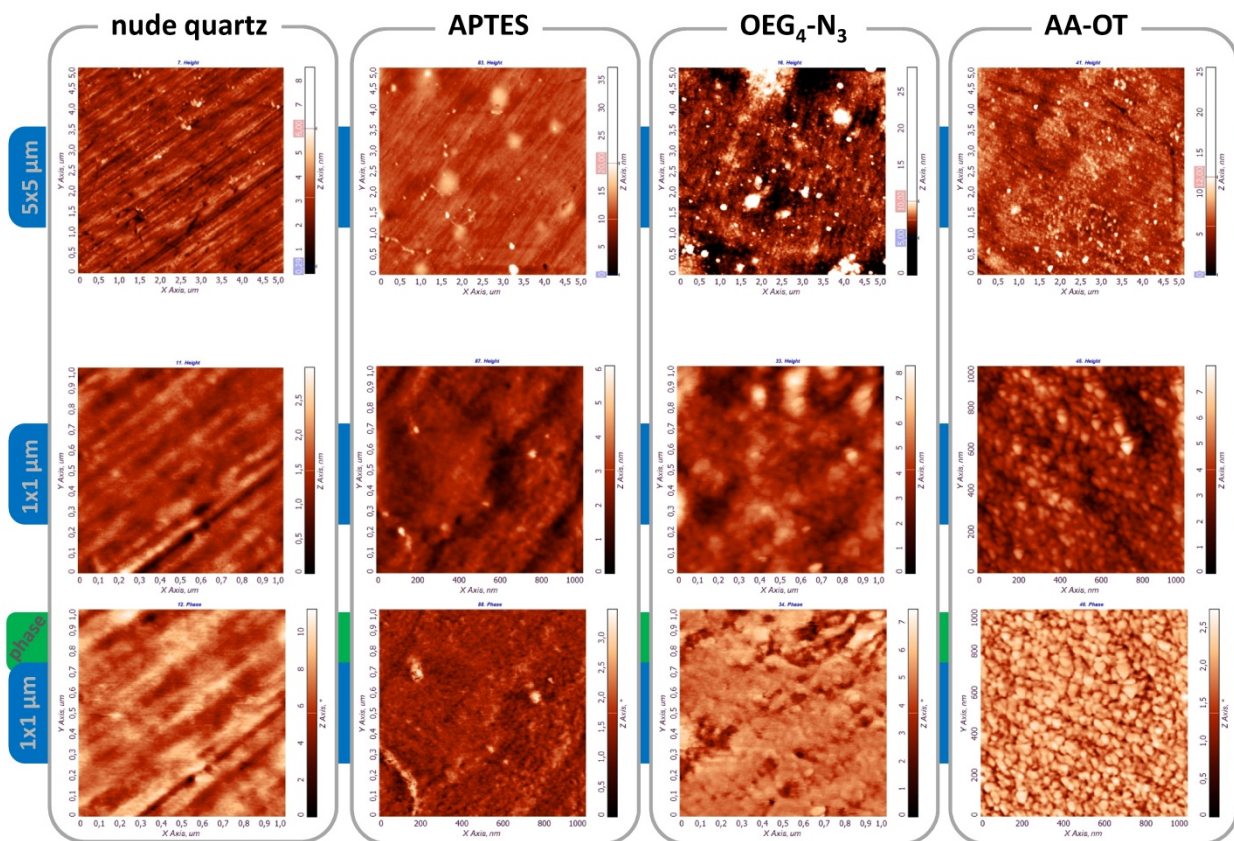
Figure 8S. AFM tapping mode analysis performed at different grafting steps, from nude quartz to AA-OT brush. The first and second rows show the morphology of 5×5 and 1×1 µm scans, respectively. The third row shows the phase contrast images of the corresponding 1×1 µm scans.
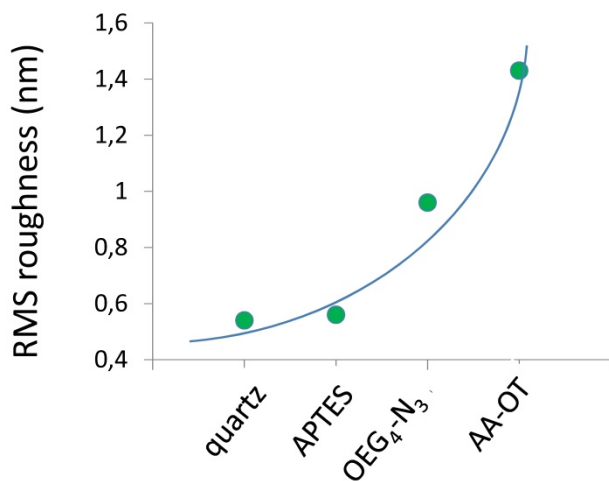

Figure 9S. RMS roughness plot. Values for different grafting steps were calculated from 5×5 µm scans.

7.3. XPS analysis

Quartz substrates were analyzed by XPS after each grafting step. The "step-by-step" variations observed in binding energy (eV) values can be explained in terms of successful formation of the covalent bonds necessary to anchor each building block of our sensing brush onto quartz surface.

In all samples, signals ascribed to the presence of Si, C, N and O are clearly detected (Figure 11S-A). As grafting proceeds, the peak attributed to nitrogen atoms (N1s) is found to be gradually shifted towards lower binding energy values (≈ 0.5 eV/step), suggesting the presence of species with not homogeneous charge distribution (Figure 11S-B). The presence of partial charges on nitrogen atoms is in agreement with the chemical transformations of the APTES $-NH_2$ group into an amide one (OEG_4-N_3 grafting step) and of the $-N_3$ residue protruding from the azido-modified surface into the triazole ring linking the oligothiophene probe (AA-OT grafting step). This latter statement is further corroborated by the appearance of sulfur signals (S2p and S2s) in the XPS spectrum of AA-OT brush. The binding energy value associated to the S2p peak (*i.e.* 165 eV) is consistent with the presence of thiophene rings on quartz surface (Figure 11S-C).
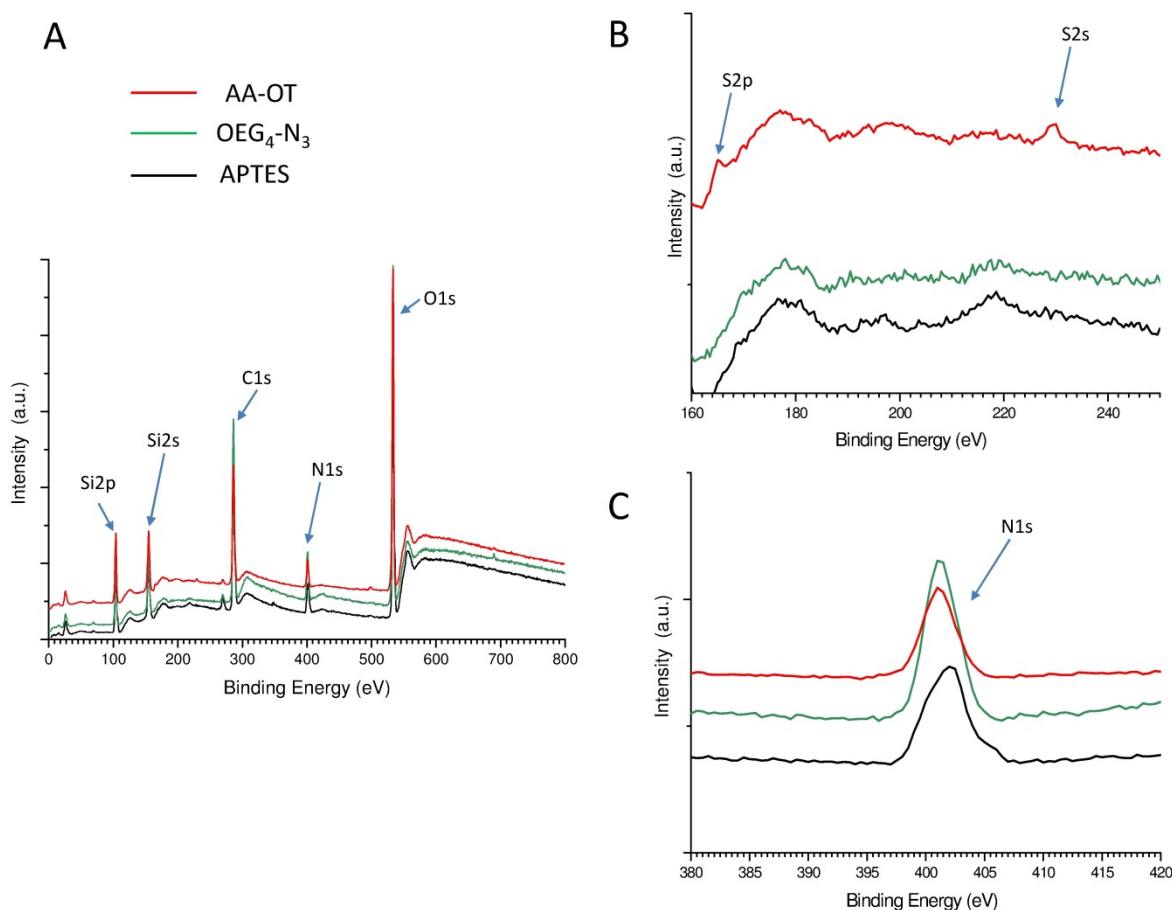

Figure 10S. A) XPS spectra of quartz substrates after each grafting step. Spectra are shifted along the y axis to aid the comparison. B) Spectral magnification showing S2p and S2s signals. C) Spectral magnification showing N1s signal.

8. X-ray analysis of the AA-OT powders

Synchrotron powder diffraction data of AA-OT are reported in Figure 10S. Three major effects can be observed, whose calculated d-spacings are 1.7 nm, 0.49 nm, and 0.40 nm respectively.

The broad bump at 16° (2θ) is clearly attributed to disordered part, largely justified by the mixtures of molecules, as recognized by MALDI-TOF analysis, constituting the examined powders. Instead, the weak peak at 4°(2θ) can be attributed to long spacings, and its broadness should be ascribed to molecules of different length.

The sharp peak at 14°(2θ) accounts for π-π stacking of molecules, enforced by H-bond formation among carboxylic groups of adjacent molecules. In fact the crystalline size along with this crystallographic direction, evaluated using line profile analysis,[1] exceeds 16 nm.
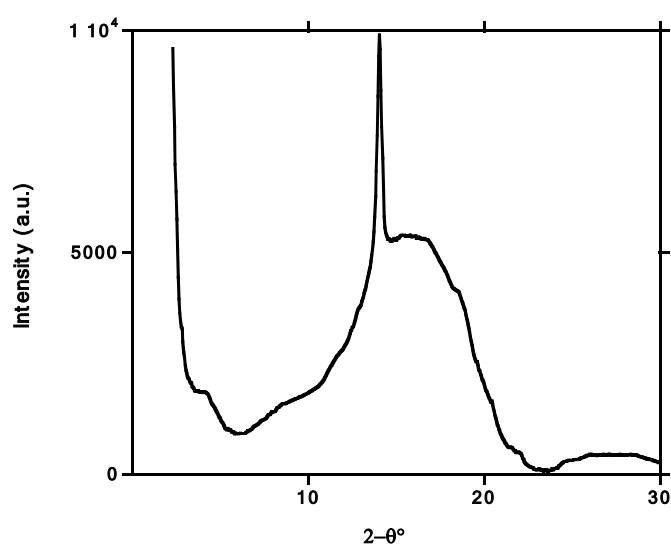
Figure 11S. XRD profile extracted from synchrotron powder data. Lambda is 0.12 nm.

REFERENCES

[1] S. Enzo, G. Fagherazzi, A. Benedetti, S. Polizzi, *J. Appl. Cryst.*, 1988, **21**, 536.